Redox Biology 64 (2023) 102788

Contents lists available at ScienceDirect

Redox Biology

journal homepage: www.elsevier.com/locate/redox

Bmal1 downregulation leads to diabetic cardiomyopathy by promoting Bcl2/IP3R-mediated mitochondrial Ca^{2+} overload

Nannan Zhang [a,b,1], Hao Yu [a,b,1], Tianzi Liu [a], Zihao Zhou [a], Bin Feng [c], Yao Wang [a], Zhiyong Qian [a], Xiaofeng Hou [a], Jiangang Zou [a,*]

[a] Department of Cardiology, The First Affiliated Hospital of Nanjing Medical University, Nanjing, China
[b] Department of Cardiology, The Affiliated Suzhou Hospital of Nanjing Medical University, Suzhou, China
[c] Department of Endocrinology, The First Affiliated Hospital of Soochow University, Suzhou, China

ARTICLE INFO

Keywords:
Diabetic cardiomyopathy
Heart failure
Bmal1
Ca^{2+} overload
Mitochondrial-associated endoplasmic reticulum membranes

ABSTRACT

Brain and muscle arnt-like protein 1 (Bmal1) is a crucial transcription factor, regulating circadian rhythm and involved in multiple heart diseases. However, it is unknown whether Bmal1 promotes diabetic cardiomyopathy (DCM) pathogenesis. The objective of this investigation was to ascertain the vital role of Bmal1 in the progression of DCM. Mice with T2D and H9c2 cardiomyoblasts exposed to high glucose and palmitic acid (HGHP) were used. Cardiomyocyte-specific knockout mouse of Bmal1 (CKB) was also generated, and cardiac Bmal1 was overexpressed in type 2 diabetes (T2D) mice using an adeno-associated virus. Bmal1 gene recombinant adenovirus was used to either knockdown or overexpress in H9c2 cardiomyoblasts. Bmal1 expression was significantly altered in diabetic mice hearts. Bmal1 downregulation in CKB and T2D mice heart accelerated cardiac hypertrophy and diastolic dysfunction, while Bmal1 overexpression ameliorated these pathological changes in DCM mice. Furthermore, DCM mice had significant mitochondrial ultrastructural defects, reactive oxygen species accumulation, and apoptosis, which could be alleviated by overexpressing Bmal1. In H9c2 cardiomyoblasts, genetic downregulation of Bmal1 or HGHP markedly decreased the binding of Bcl2 to IP3R, thus increasing Ca^{2+} release to mitochondria through mitochondria-associated endoplasmic reticulum membranes. Importantly, chromatin immunoprecipitation revealed Bmal1 could bind directly to the *Bcl2* gene promoter region. Bmal1 overexpression augmented the Bmal1/Bcl2 binding, enhancing the inhibition of Bcl2 on IP3R activity, thus alleviating mitochondrial Ca^{2+} overload and subsequent cell apoptosis. These results show that Bmal1 is involved in the DCM development through Bcl2/IP3R-mediated mitochondria Ca^{2+} overload. Therapy targeting the circadian clock (Bmal1) can treat DCM.

1. Introduction

Diabetes is a major health concern on a global scale, with cardiovascular complications being a primary defect in the pathology of this disease. Type 2 diabetes (T2D) accounts for 90–95% of the total diabetes cases and can increase the incidence of heart failure (HF) regardless of age or concomitant comorbidities, including coronary artery disease, cardiac valve disease, and dyslipidemia [1,2]. Individuals diagnosed with HF are also susceptible to an elevated likelihood of developing diabetes [3]. Diabetic patients are initially characterized by increased myocardial stiffness, cardiac hypertrophy, diastolic dysfunction, myocardial fibrosis, and preserved systolic contraction [4,5], a clinical condition referred to as diabetic cardiomyopathy (DCM). Although multifactorial mechanisms, including energy metabolism, oxidative stress, inflammatory reaction, and elevated myocardial cell apoptosis, promote DCM development, the pathomechanisms underlying this disease are unclear [3,5]. As a result, there is no effective treatment for the prevention of DCM or for reversing the underlying molecular changes.

The rhythmicity, automaticity, and every cardiac cycle use a lot of energy produced via oxidative phosphorylation within mitochondria [6,7]. Mitochondria-mediated apoptosis is increased in heart tissue due to reactive oxygen species (ROS) overproduction, mitochondrial ultrastructural defects, mitochondrial permeability transition pore (mPTP) opening, diminished mitochondrial membrane potential (MMP, $\Delta\Psi m$),

* Corresponding author. Department of Cardiology, the First Affiliated Hospital of Nanjing Medical University, 300 Guangzhou Rd, Nanjing, 210029, China.
E-mail address: jgzou@njmu.edu.cn (J. Zou).
[1] Nannan Zhang and Hao Yu contributed equally to this work.

https://doi.org/10.1016/j.redox.2023.102788
Received 20 January 2023; Received in revised form 11 June 2023; Accepted 15 June 2023
Available online 20 June 2023

and apoptotic stimuli, for instance, cytochrome C (Cyt-C), the second mitochondria-derived stimulator of caspases (Smac) leaking to cytosol in DCM [3,8]. Ca^{2+} signaling in mitochondria regulates mitochondrial metabolism and promotes cell death [9]. Furthermore, increased and reduced mitochondrial Ca^{2+} levels are involved in mitochondrial dysfunction and increased ROS production in DCM [5,10]. The concentration of Ca^{2+} in mitochondria depends on the pathways across the endoplasmic reticulum (ER), mitochondria-associated ER membranes (MAMs), and mitochondria [9]. Disordered Ca^{2+} transfer in DCM patients through MAMs significantly induces intrinsic mitochondrial apoptosis [11]. Although various proteins, such as mitofusion (Mfn), inositol 1,4,5-triphosphate receptor-glucose-regulated protein 75-voltage-dependent anion-selective channel (IP3R-Grp75-VDAC) are involved in regulating Ca^{2+} transfer in MAMs, the above regulatory mechanisms are unclear [11,12]. Therefore, further studies should comprehensively explore MAMs and mitochondrial Ca^{2+} for an in-depth insight into the mechanism of DCM.

The circadian system is critical in mammalian homeostasis, regulating responses to 24 h environmental cycles [13–15]. Mammals are known to have both central and peripheral clocks. Situated at the suprachiasmatic nucleus (SCN) in the brain, the central clock functions as the primary pacemaker responsible for synchronizing the clocks present within peripheral tissues and other brain regions. Peripheral clocks are located within different regions, including the liver, pancreas, adipose, heart, etc [14,15]. The generation of circadian rhythms occurs at the cellular level through the utilization of transcription-translation feedback loops (TTFLs). Two transcriptional stimulators (brain and muscle arnt-like protein 1 (Bmal1) and the circadian locomotor output cycles kaput protein (Clock)) form the main activator heterodimers that promote the two suppressors Period (Per1, 2, 3) and Cryptochrome (Cry1,2) expression, which later dimerizes and inhibit Bmal1/Clock activity [14,15]. Bmal1 is essential in autoregulatory TTFLs, which generate the rhythmic transcription of output genes [13,16]. Furthermore, disruption of Bmal1 activity promotes the pathogenesis of metabolic diseases [17]. A recent study reported that Bmal1 expression is substantially decreased and is associated with altered rhythmic mitochondrial metabolism in skeletal muscle from T2D patients [18]. The expression of multiple insulin signaling and metabolic factors within the heart of mice is altered due to the circadian clock genetic disturbance through the cardiomyocyte-specific knockout mice of Bmal1 (CKB) [19]. Mitochondria are central in metabolic integration, indicating that mitochondrial function may be associated with circadian rhythms in one or several mechanisms [20,21]. However, it is unknown whether Bmal1 disruption is associated with DCM development. Besides, the underlying mechanisms related to mitochondrial Ca^{2+} are unclear.

Given the above findings, we hypothesized that the circadian gene Bmal1 participates in the pathogenesis of DCM by regulating mitochondrial Ca^{2+} homeostasis in T2D mice. Therefore, this study may provide new insights into mechanism-based DCM therapeutics.

2. Materials and methods

2.1. Experimental animal

Throughout the experiment, total 87 male mice (Gempharmatech Co., Ltd., Jiangsu) from a C57BL/6j background were used and all mice were housed in the laboratory animal center of Nanjing Medical University under constant humidity and temperature and access to water, and food was provided without any restrictions. All the mice were kept in a controlled condition with a strict 12/12 h light/dark cycle (LD 12:12), and the light was switched on from 6:00 a.m. (zeitgeber time 0, ZT0) to 6:00 p.m. (ZT12). At the end of the study, mice were anesthetized using 1%–2% isoflurane and subsequently experienced death through cervical dislocation.

The study's experimental methods were conducted followed the protocols outlined in the Guide for the Care and Use of Laboratory Animals, as referenced by the US National Institutes of Health (8th edition, revised, 2011). The Laboratory Animal Welfare & Ethics Committee (IACUC) of Nanjing Medical University granted the approval for this investigation (Ethics No. 2005052).

2.2. Construction of T2D model

A high-fat diet (HFD, 60% fat of total kcal) was administered to the mice, along with an intraperitoneal injection of streptozotocin (STZ) as previously described with minor modifications to established T2D models [22]. Briefly, after 11 weeks of HFD, the mice were subjected to three consecutive days of STZ (40 mg/kg) injections via the intraperitoneal (Dissolving STZ using 0.1 M pre-cooled citrate buffer, immediately before application, pH 4.5). Meanwhile, mice intraperitoneally injected with citrate buffer served as controls (CON, n = 15). Mice with fasting tail vein blood sugar level above 16.7 mmol/L were diagnosed as diabetic and proceeded to feed on HFD until they were sacrificed at 31 weeks of age (HFD + STZ, n = 15). Three mice were killed every 6 h from 6 a.m. to 6 a.m. the following day (ZT0, 6, 12, 18, 24) to assess the circadian expression of proteins in the heart. Additionally, male *db/db* mice (31 weeks old) were also used as T2D models to confirm the circadian gene changes in the diabetic heart (db/db, n = 9).

2.3. Construction of cardiomyocyte-specific Bmal1 knockout mice and cardiac overexpression of Bmal1 in T2D mice

$Bmal1^{flox/flox}$ mice were bred with Myh6-cre mice (Jackson Labs, USA) for multiple generations to generate $Cre^{+/-}$. $Bmal1^{flox/flox}$/α-MHC-$Cre^{+/-}$ mice were used for constructing Bmal1 knockout (CKB, n = 12) mice via intraperitoneal injection of tamoxifen (TMX, 50 mg/kg) for five consecutive days. $Bmal1^{flox/flox}$ littermates with TMX administration served as controls (CON, n = 12). Detailed methods are available in the online Supplementary Material.

T2D mice were induced by HFD and STZ combination as described above. The adeno-associated virus type 9 (AAV9) driven by cardiomyocytes-specific promoter cTNT: 3Flag-Bmal1 (AAV9: cTNT-Bmal1) for cardiac-specific Bmal1 overexpression and control AAV9 (AAV9: cTNT-Ctrl) were sourced from Genechem Company (CN). The T2D mice were injected with AAV9: cTNT-Ctrl or AAV9: cTNT-Bmal1 via tail vein (2×10^{12} vg/kg; T2D + AAV-Ctrl, n = 12; T2D + AAV-Bmal1, n = 12). The flow chart of the animal experiment is according to Fig. 2A.

2.4. Culture and treatment of H9c2 cardiomyoblasts

Rat H9c2 cardiomyoblasts (Zhong Qiao Xin Zhou Biotechnology, CN) were maintained within DMEM that include penicillin (100 U/mL), streptomycin (100 μg/mL) and 10% fetal bovine serum. H9c2 cardiomyoblasts underwent incubation in standard medium (CON, 5.5 mM D-glucose) or high glucose and palmitic acid (PA) medium (HGHP, 33.3 mM D-glucose, 100 μM PA) for a period of 48 h. Intrinsic rhythms were synchronized using a well-established serum-shock (50% horse serum) approach to investigate the circadian expression of Bmal1 [23]. Detailed synchronization methods are available in the online Supplementary Material. Recombinant adenovirus carrying shRNA for Bmal1 knockdown (Ad-shBmal1) and overexpression (Ad-Bmal1) were designed by Genechem Company (CN). Adenovirus carrying nontarget shRNA or a blank gene were used as controls (Ad-shCtrl and Ad-Ctrl, respectively). The H9c2 cardiomyoblasts were starved with no serum media for 6–8 h, then transfected with the corresponding adenoviruses for 12 h, followed by standard or HGHP media for another 48 h. The sequences of Ad-shBmal or Ad-shCtrl are shown in Supplementary Table 1. BIRD-2 peptide (LifeTein, USA), specifically disrupting the Bcl2/IP3R complex, was used in HGHP-treated H9c2 cells for 12 h (20 μM).

2.5. Echocardiography

The mice were anesthetized with 1% isoflurane for cardiac function examination with echocardiography every four weeks. The VEVO 3100 echography device (VisualSonics, Toronto, Canada) was utilized to perform a high-frequency ultrasound for M-mode, pulse wave Doppler (PWD), and tissue Doppler (PWTD) imaging. The mice were put in a supine position above a heating platform with a consistent temperature (37.0 ± 0.5 °C). M-mode tracing was acquired through the left ventricular (LV) short-axis view at the papillary muscles level for evaluating LV wall thickness, mass, systolic function, and other parameters. PWD and PWTD recordings have been gathered from the apical four-chamber view for measuring E/A, E/e', LV iso-volumetric relaxation time (IVRT), and LV myocardial performance index (LV MPI). All evaluations were operated with a single observer who had no access to the mice's identity, and all parameters were averaged from 3 cardiac cycles. The visualization of the above data was performed utilizing The VEVO 3100 software (version 1.5.0).

2.6. Transmission electron microscopy

Transmission electron microscopy (TEM) provided by (Hitachi High-Technologies Europe GmbH) was utilized to examine the ultrastructure of myocardial cells and H9c2 cardiomyoblasts. The total ER attached to mitochondria was normalized to the total ER perimeter for MAMs quantification. The quantification of the mitochondrial ER proximity relationship was performed utilizing Image J software (National Institutes of Health). Detailed methods are available in the online Supplementary Material.

2.7. Flow cytometry analysis

Live H9c2 cardiomyoblasts were incubated with MitoSOX™ red mitochondrial superoxide indicator (Invitrogen, USA) or Rhod 2 a.m. probe (Yeasen, CN) for the detection of mitochondrial ROS or mitochondrial Ca^{2+} level, respectively. Annexin V-APC/7-AAD apoptosis identification kit (Keygene, CN) was employed to identify the cell apoptosis levels. Flow cytometry (FCM) was then utilized to estimate the fluorescence intensity of the suspended single cells. FlowJo software was used to measure mean fluorescence intensity (MFI). Detailed methods are available in the online Supplementary Material.

2.8. Mitochondrial fluorescent staining

Live H9c2 cardiomyoblasts in 24-well plates were incubated with TMRE (Beyotime, CN), MitoSOX™, and Rhod 2 a.m. probes following standard instructions for the detection of MMP (ΔΨm), ROS, and Ca^{2+}, respectively. Rhod 2 a.m. may be distributed within non-mitochondrial chambers contained inside the cell. Thus, MitoTracker Green was used to co-stain mitochondria, while MitoTracker Green/Rhod 2 a.m.-dual positive areas were used to calculate mitochondrial Ca^{2+} with the microscope. The cell nuclei were subjected to a restaining process utilizing 4,6-diamidino-2-phenyl (DAPI) where necessary. For MAMs, ER and mitochondria were simultaneously labeled via Mito-Tracker Green and ER-Tracker Red in H9c2 cardiomyoblasts. The MFI and the mean grey values (MGV) were analyzed utilizing Image J. For the purpose of determining the degree of colocalization among the fluorophores, the Pearson correlation coefficient was calculated. Detailed methods are available in the online Supplementary Material.

2.9. Co-immunoprecipitation

The treated H9c2 cardiomyoblasts were collected and lysed with lysis buffer (Beyotime, CN) for co-immunoprecipitation (CoIP) assay. The proteins were incubated with IP3R antibody (1:50, A21471, ABclonal) overnight at a temperature of 4 °C, subsequent by incubation with PureProteome™ Protein A Magnetic Beads (LSKMAGG10, Millipore Corp, USA). Specifically, 25 μL of suspended PureProteome™ Magnetic Bead slurry was supplemented to a microcentrifuge tube and hydrated via 500 μL binding buffer by vigorous vortexing for 10 s. Adding 150 μL of the antibody-antigen sample to the beads and the mixture was incubated for a period of 4 h with rotating at a temperature of 4 °C. Afterwards, beads underwent hydration four times by lysis buffer on a rotator for a period of 1 h at a temperature of 4 °C and underwent a boiling process within 40 μL of sample loading buffer (P0015B, Beyotime, China) and examined via immunoblotting.

2.10. Chromatin immunoprecipitation assay

The Chromatin Immunoprecipitation Kit (9003, Cell Signaling Technology, USA) was utilized for performing chromatin immunoprecipitation (ChIP) assays following the manufacturer's protocol. Summarily, the nucleic acids and DNA-binding proteins were crosslinked. A total of 10^7 cellular chromatin samples underwent sonication, resulting in fragments ranging from 200 to 500 bp in ChIP dilution buffer. Then the DNA fragments were immunoprecipitated in dilution buffer using Bmal1 antibody at 1:50 dilution (or negative control IgG antibody, 1:50) and subsequently incubated at a temperature of 4 °C overnight. The antibody complexes were enriched using immunomagnetic beads and de-crosslinked to release DNA fragments at 65 °C in elution buffer for 5 h, after which DNA was isolated. Real-time quantitative PCR (qRT-PCR) was conducted using primers specific to the Bmal1 predicted binding site (E-Box) on the *Per1* and *Bcl2* promoters. The sequences of *Per1* and *Bcl2* primers are exhibited in Supplementary Table 2.

2.11. Statistical analysis

The data are presented as mean ± standard deviation (SD). The data normality was evaluated utilizing the Shapiro-Wilk test, and all data sets in the article passed the normality distribution test. As for homoscedasticity, the Bartlett test was utilized to examine the variance homogeneity of the data, and the corresponding population variances are equal. Standard student t-test was used for comparisons between two groups. One-way ANOVA (one variable), or two-way ANOVA (two variables) was employed to assess variances in multi-group comparison, subsequent by Bonferroni post-hoc tests. For repeated measures data, using two-way repeated measures ANOVA analyzed differences. P values < 0.05 were proved to be statistically significant. All statistical analyses were conducted utilizing SPSS 20.0 statistical software (IBM Corp., USA). GraphPad Prism 5 and Adobe Illustrator software were utilized for graphing.

3. Results

3.1. Myocardial Bmal1 expression is reduced and arrhythmic in T2D mice

Transcription factors Bmal1 and Clock are core TTFLs protein components. Therefore, we focused on the circadian rhythm of Bmal1 and Clock expression in the hearts of T2D mice. Compared with CON, rhythmicity and oscillation of Bmal1 mRNA were significantly attenuated at all ZT points, while those of Clock mRNA were not affected (Fig. 1A and B). The protein expression changes were consistent with the mRNA changes (Fig. 1C–E). IHC staining of Bmal1 in myocardial tissues mice further confirmed the above findings (Fig. 1F and G). In addition, glucose metabolism parameters such as serum insulin, fasting blood glucose, glucose tolerance test, and lipid profiles were determined in both HFD + STZ and *db/db* mice (Suppl. Figs. 1A–E). Cardiac function of mice was assessed via echocardiography. Diabetic mice had thickened LV wall (Suppl. Figs. 1F and G) and impaired diastolic function, indicated by significantly decreased E/A, increased E/e', as well as IVRT (Suppl. Figs. 1H and I). Compared with CON group, BNP and ANP serum

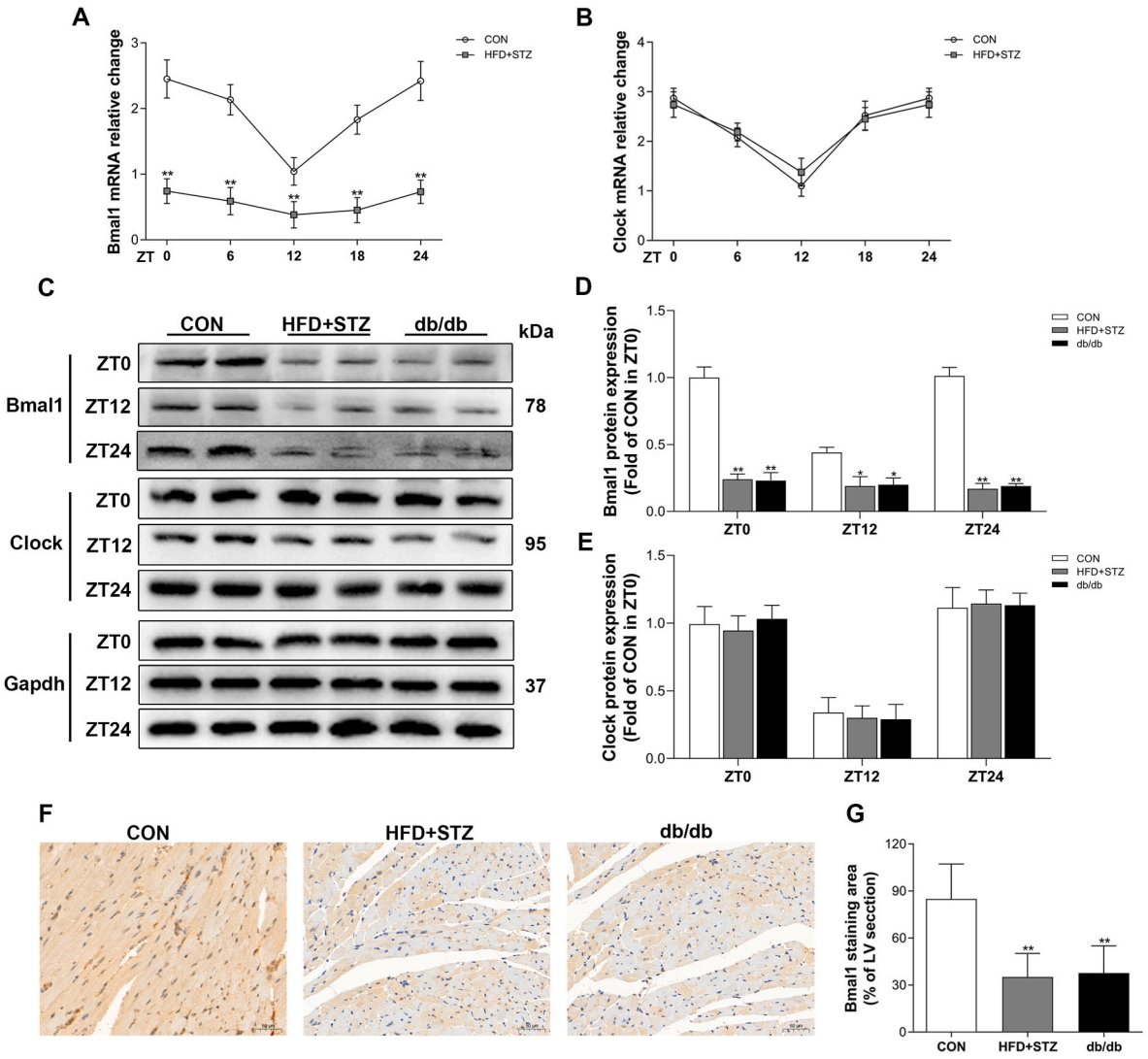

Fig. 1. The expression and rhythmicity of Bmal1 were significantly downregulated in T2D mice heart. (A, B) Bmal1 and Clock mRNA levels at different ZT points (0–24). n = 3 mice per group per ZT point. (C–E) Protein expression level of Bmal1 and Clock at ZT0, ZT12 and ZT24 as determined by western blots. n = 3 mice per group per ZT point. (F, G) Immunohistochemical staining of Bmal1 protein in left ventricular myocardium. Scale bar: 50 μm. If not specifically stated, n = 5 to 7 mice per group. Data are presented as the mean ± SD. Statistical significance was determined using two-way repeated measures ANOVA (A, B, D, E) or one-way ANOVA (G) with Bonferroni post-hoc tests. $^{*}P < 0.05$ and $^{**}P < 0.01$ vs. CON.

levels in T2D mice were markedly higher (Suppl. Fig. 1J). However, as for systolic parameters, there was no statistical difference in fraction shortening (FS) or ejection fraction (EF) among the three groups (Suppl. Fig. 1K).

3.2. *Bmal1 deficiency leads to cardiac hypertrophy and diastolic dysfunction in T2D mice*

Cardiac-specific knockdown or overexpression of Bmal1 was induced to investigate the effect of Bmal1 disruption in mouse hearts. The flow chart of the experiment is presented in Fig. 2A. HE staining and echocardiography showed cardiac hypertrophic remodeling in T2D mice, reflected by the significantly thickened interventricular septal wall (IVST) (Fig. 2B and C), LV anterior wall in systole/diastole (LVAWs/d) and posterior wall in diastole (LVPWd) (Table 1). However, Bmal1 overexpression in T2D + AAV-Bmal1 reduced the thickened IVST (Fig. 2B and C), LVAWs/d, and LVPWd (Table 1). Consistently, Bmal1 overexpression decreased LV mass and relative heart weight (heart weight/body weight, HW/BW, HW/tibial length, TL) (Table 1). Additionally, LV end-systolic dimension (LVESD) was dilated in CKB and T2D control mice, but not LV end-systolic dimension (LVEDD). However, this dilation was relieved in the T2D + AAV-Bmal1 group (Table 1). WGA staining indicated Bmal1 overexpression significantly reduced the cross-section area (CSA) of cardiomyocytes in the diabetic mice (Fig. 2D and E).

Masson staining also revealed that genetically knockdown or HFD + STZ induced downregulation of Bmal1 significantly induced myocardium fibrosis. However, cardiac-specific overexpression of Bmal1 significantly alleviated fibrotic remodeling in diabetic mice (Fig. 2F and G). Moreover, echocardiography detected distinct diastolic dysfunction in CKB and T2D mice, mainly indicated as decreased E/A and increased E/e' and IVRT. However, Bmal1 upregulation significantly improved diastolic dysfunction of the diabetic heart (Table 1). For systolic function, no remarkable differences were found among the four groups in FS, EF, and cardiac output (CO). Representative images of echocardiography are shown in Fig. 2H.

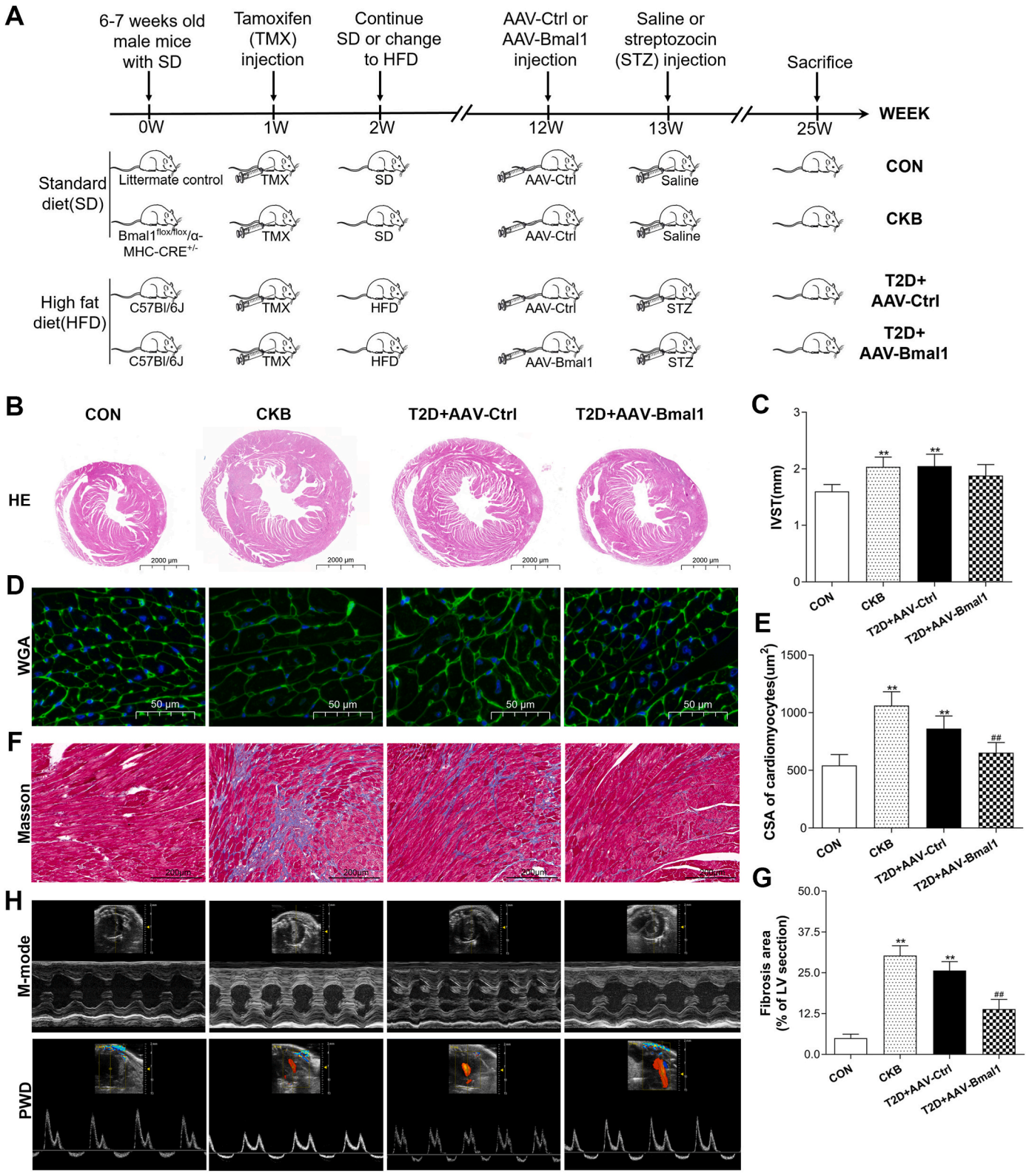

Fig. 2. Bmal1 deficiency induced cardiac hypertrophy and fibrosis in DCM and cardiac Bmal1 overexpression alleviated these changes. (A) The flow chart of animal experiments. (B, C) HE staining of left ventricle myocardium and IVST measurements. Scale bar: 2000 μm. (D, E) WGA staining of left ventricle myocardium and CSA of cardiomyocytes. Scale bar: 50 μm. (F, G) Masson staining of left ventricle fibrosis and fibrosis area proportion. Scale bar: 200 μm. (H) Representative M-mode and PWD echocardiography images. n = 5 to 7 mice per group. Data are presented as the mean ± SD. Statistical significance was determined using two-way ANOVA with Bonferroni post-hoc tests. $^{**}P < 0.01$ vs. CON. $^{\#\#}P < 0.01$ vs. T2D + AAV-Ctrl.

Table 1
Comparison of weight and echocardiographic parameters in each group.

	CON	CKB	T2D + AAV-Ctrl	T2D + AAV-Bmal1
Weight				
BW (g)	30.92 ± 1.16	33.50 ± 2.01**	28.80 ± 1.69*	29.33 ± 1.83
HW (g)	0.13 ± 0.02	0.23 ± 0.04**	0.21 ± 0.05**	0.16 ± 0.02$^{\#}$
HW/BW (g/kg)	4.10 ± 0.79	6.95 ± 1.60**	7.27 ± 1.44**	5.62 ± 0.50$^{\#}$
HW/TL (g/cm)	0.08 ± 0.01	0.15 ± 0.03**	0.14 ± 0.03**	0.10 ± 0.01$^{\#\#}$
Echocardiography				
HR (b.p.m)	431.12 ± 32.35	508.16 ± 64.10**	577.07 ± 52.59**	535.35 ± 47.51
LVESD (mm)	1.78 ± 0.26	2.22 ± 0.34**	2.18 ± 0.35*	1.85 ± 0.13
LVEDD (mm)	3.46 ± 0.26	3.53 ± 0.26	3.51 ± 0.35	3.33 ± 0.10
LVAWs (mm)	1.55 ± 0.20	1.88 ± 0.16**	2.02 ± 0.11**	1.69 ± 0.19$^{\#\#}$
LVAWd (mm)	0.97 ± 0.13	1.37 ± 0.12**	1.48 ± 0.15**	1.13 ± 0.16$^{\#\#}$
LVPWs (mm)	1.45 ± 0.15	1.53 ± 0.11	1.65 ± 0.13*	1.42 ± 0.16$^{\#\#}$
LVPWd (mm)	0.91 ± 0.08	1.15 ± 0.08**	1.19 ± 0.08**	0.97 ± 0.09$^{\#\#}$
LV mass (g)	0.12 ± 0.01	0.19 ± 0.04**	0.20 ± 0.04**	0.13 ± 0.02$^{\#\#}$
E/A	1.67 ± 0.32	1.18 ± 0.13**	1.16 ± 0.08**	1.43 ± 0.19$^{\#}$
E/e'	26.12 ± 6.29	36.42 ± 6.06*	37.18 ± 7.89*	28.49 ± 7.51$^{\#}$
IVRT (ms)	18.63 ± 3.24	27.11 ± 5.16**	25.89 ± 6.57**	19.88 ± 3.20$^{\#}$
LV MPI	0.48 ± 0.09	0.75 ± 0.05**	0.76 ± 0.19**	0.59 ± 0.11$^{\#}$
LVFS (%)	39.20 ± 4.80	39.48 ± 4.90	40.52 ± 6.62	39.47 ± 4.94
LVEF (%)	60.04 ± 5.08	58.67 ± 5.91	59.51 ± 2.50	57.40 ± 3.57
CO (mL/min)	21.09 ± 4.47	20.54 ± 2.77	20.59 ± 4.54	18.50 ± 2.24

Bmal1 reduction led to cardiac hypertrophy and diastolic dysfunction in T2D mice. Cardiac overexpression of Bmal1 could alleviate these pathological changes. BW, body weight; HW, heart weight; TL, tibia length; HR, heart rate; b.p.m, beat per minute; LV, left ventricular; LVESD, LV end systolic dimension; LVEDD, LV end diastolic dimension; LVAW, LV anterior wall thickness; LVPW, LV posterior wall thickness; IVRT, iso-volumetric relaxation time; LV MPI, LV myocardial performance index; LVFS, LV fractional shortening; LVEF, LV ejection fraction; CO, cardiac output. The 's' and 'd' after the acronyms indicate end-systole and end-diastole, respectively. Data are presented as the mean ± SD. Statistical significance was determined using two-way ANOVA with Bonferroni post-hoc tests. $^{*}P < 0.05$ and $^{**}P < 0.01$ vs. CON, $^{\#}P < 0.05$ and $^{\#\#}P < 0.01$ vs. T2D + AAV-Ctrl.

3.3. Bmal1 overexpression ameliorates diabetes-induced mitochondria-mediated apoptosis

Apoptosis is mainly induced by the caspases, which proceed through two different signaling pathways: intrinsic (mitochondria-mediated) and extrinsic (death receptor-mediated) pathways (Suppl. Fig. 2A). In this study, significant mitochondrial injuries and intrinsic cell apoptosis occurred in DCM mice (Suppl. Figs. 2B–K). Furthermore, Bmal1 was downregulated in the CKB and T2D groups (Fig. 3A and B). AAV-mediated cardiac-specific expression successfully restored Bmal1 content in the heart of diabetic mice. Lack of Bmal1 significantly enhanced poly ADP-ribose polymerase (c-PARP) cleaved levels and caspases (c-Caspase9/c-Caspase3) in CKB and T2D + AAV-Ctrl mice (Fig. 3A, C). Moreover, the contents of Cyt-C and Smac were significantly decreased in mitochondria and increased in the cytoplasm, indicating impaired mitochondrial membrane and leakage of pro-apoptotic factors from mitochondria to cytoplasm occur in myocardium without Bmal1 (Fig. 3A, D, E). Notably, exogenous re-expression of Bmal1 deactivated the above apoptotic process in the hearts of T2D + AAV-Bmal1 mice. In addition, TUNEL and ROS staining showed that cardiomyocyte apoptosis and ROS production increased in T2D mice. However, cardiomyocyte apoptosis and ROS production were significantly relieved after restoring the expression of cardiac Bmal1 (Fig. 3F–I).

Myocardial tissue was examined using transmission electron microscopy to assess the mitochondrial morphological changes caused by Bmal1 deficiency. Mitochondrial swelling, vacuolation and cristae fragmentation were detected in cardiomyocytes of CKB and T2D control mice (Fig. 3J-L). However, upregulation of cardiac Bmal1 by AAV vectors strongly attenuated these abnormal morphologies. Interestingly, the formation of MAMs elevated in the diabetic mice's heart. Nevertheless, Bmal1 overexpression significantly decreased the proximity between ER and mitochondria in cardiomyocytes (Fig. 3M).

3.4. Loss of Bmal1 expression exacerbates mitochondrial damages and apoptosis in vitro

Contrasted to the control group, mRNA levels of Bmal1 were notably decreased in HGHP-treated H9c2 cardiomyoblasts at all time points after serum shock (Fig. 4A). Furthermore, knockdown with shRNA target Bmal1 or HGHP treatment both substantially increased the levels of apoptotic indicators (c-PARP/Caspase9/Caspase3) in cells (Fig. 4B–D). Simultaneously, Cyt-C and Smac contents were considerably elevated in the cytosol and decreased in mitochondria (Fig. 4B, E, F). Bmal1 deficiency promoted apoptosis in Ad-shBmal1 transfected and HGHP-treated H9c2 cells (Fig. 4G and H). Importantly, replenishing Bmal1 via adenovirus vectors effectively blocked the aforementioned cellular apoptotic response. Bmal1 overexpression significantly alleviated mitochondrial morphological damages, such as swelling, number loss, and vacuolation, which occurred in CON-Ad-shBmal1 and HGHP-Ad-Ctrl cells, similar to *in vivo* experiments (Fig. 4I-L).

Besides, mitochondrial membrane potential (MMP, ΔΨm) was determined using TMRE probe and quantified using a fluorescence microscope and microplate reader. Bmal1 knockdown or HGHP-induction in H9c2 cells, significantly decreased ΔΨm, while Bmal1 upregulation increased the ΔΨm (Fig. 5A–C). MitoSOX staining and FCM analysis demonstrated that Bmal1 downregulation could induce ROS overproduction in mitochondria. However, the exogenous viral vector upregulated Bmal1 strongly suppressed mitochondrial ROS generation in cells (Fig. 5D–G). Moreover, polyethylene glycol-superoxide dismutase (PEG-SOD) was used to clarify the association between Bmal1 and mitochondrial ROS. As shown in Suppl. Figs. 3A and C, fluorescence microscopy results showed that compared with CON-Ad-shBmal1, MGV of MitoSOX in CON-Ad-shBmal1-PSOD was significantly decreased. Likewise, MGV in HGHP-Ad-Ctrl-PSOD was markedly lower than that in HGHP-Ad-Ctrl. FCM indicated MitoSOX MFI changes among groups were similar to MGV (Suppl. Figs. 3B and D). Additionally, malondialdehyde (MDA) levels in CON-Ad-shBmal1 and HGHP-Ad-Ctrl cells were significantly increased while overexpression of Bmal1 in HGHP-induced cells markedly reduced the MDA levels (Fig. 5H).

3.5. Bmal1 overexpression relieves mitochondrial Ca^{2+} overload and MAMs formation in H9c2 cardiomyoblasts

Mitochondrial Ca^{2+} overload is closely related to mitochondrial damage, apoptosis, cardiac remodeling, and development of HF [24]. In this study, mitochondrial Ca^{2+} levels were monitored using Rhod 2 a.m. probe [25,26]. Mitochondrial Ca^{2+} content was significantly increased in CON-Ad-Bmal1 and HGHP-Ad-Ctrl cells contrasted with the control group. Nevertheless, this change was significantly reversed in Bmal1-overexpressed H9c2 cells (Fig. 6A, C). FCM analysis showed similar results (Fig. 6B, D). Furthermore, Bmal1 downregulation enhanced MAMs formation, indicated by increased colocalization of ER and mitochondria fluorescent staining in Ad-shBmal1-transfected and HGHP-treated cells. However, Bmal1 upregulation significantly weakened the couplings between mitochondria and ER (Fig. 6E and F).

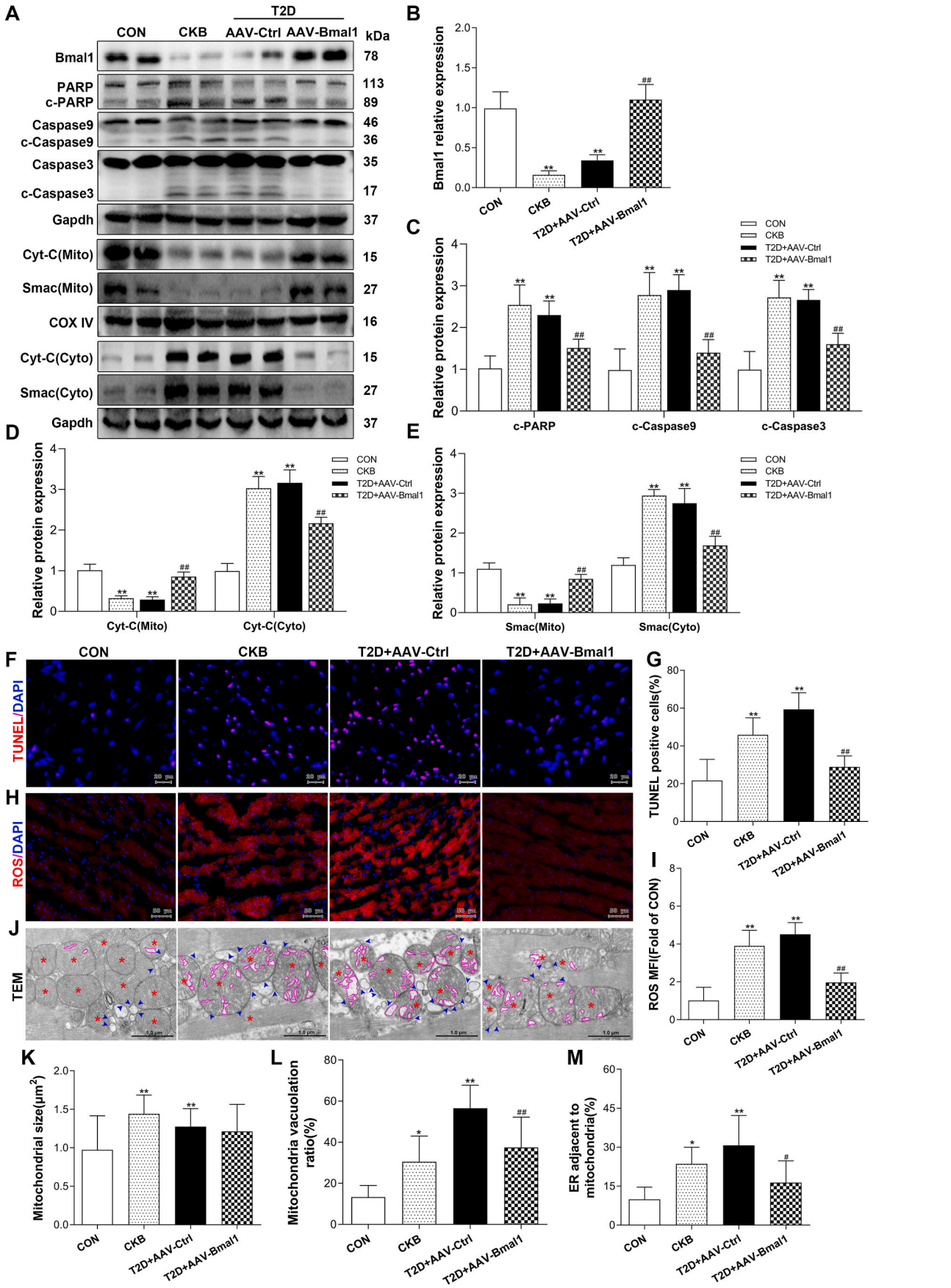

(caption on next page)

Fig. 3. Restoration of Bmal1 expression ameliorated mitochondrial damage and apoptosis. (A) Western blots results showing expression of Bmal1 and proteins associated with mitochondria-mediated apoptosis. (B, C) Quantification analysis of Bmal1, c-PARP and c-Caspase9/3 protein levels in whole tissue lysates. Presenting as fold changes relative to the CON group. (D, E) Quantification analysis of Cyt-C and Smac protein levels in mitochondria lysates or cytosol lysates. Presenting as fold changes relative to the CON group. (F, G) TUNEL staining was conducted to explore apoptosis of LV cells and the positive cells ratio was calculated. Scale bar: 20 μm. (H, I) ROS fluorescence labelling of LV and quantitation of ROS MFI. Scale bar: 50 μm. (J) Representative TEM images of mitochondria in LV cardiomyocytes. Scale bar: 1 μm. Red asterisk, mitochondria; purple circle, vacuole; blue triangle, ER adjacent to mitochondria contacts. n = 3 mice per group. (K, L) Quantification of mitochondrial size and vacuolation. Total 60 mitochondria were calculated per group. (M) The ratio of ER adjacent to mitochondria in cardiomyocytes. Total 40–60 ER adjacent to mitochondria contacts were calculated per group. If not specifically stated, n = 5 to 7 mice per group. Data are presented as the mean ± SD. Statistical significance was determined using two-way ANOVA with Bonferroni post-hoc tests. $^{*}P < 0.05$ and $^{**}P < 0.01$ vs. CON. $^{\#}P < 0.05$ and $^{\#\#}P < 0.01$ vs. T2D + AAV-Ctrl.

Similarly, TEM imaging showed that the ER-mitochondria coupling structures percentage elevated in the absence of Bmal1, while Bmal1 expression significantly increased the spatial distance between the two organelles (Fig. 6G and H).

3.6. Bmal1 downregulation relieves the inhibitory effect of Bcl2 on IP3R to promote Ca^{2+} transfer through MAMs

As the mitochondria-ER tethering complexes core subset, IP3R-Grp75-VDAC consists of IP3Rs in the ER and VDAC in the mitochondria outer membrane. Mitofusion2 (Mfn2) can form complexes with Mfn1 or Mfn2 on the mitochondrial surface, tethering ER to mitochondria tightly [11,27]. Therefore, we further explored potential targets of Bmal1 that regulate MAMs formation and mitochondrial Ca^{2+} levels. As shown in Fig. 7A and Suppl. Fig. 4A, the protein expression of Grp75, VDAC, and Mfn2 was significantly increased following Bmal1 knockdown or HGHP induction, and inhibited under HGHP-Ad-Bmal1 conditions, and this was ascribed to the restoration of Bmal1 content. Of note, there were no detectable changes in IP3R among the groups, a key channel for MAMs-mediated Ca^{2+} transport [28,29] (Fig. 7A and B). Therefore, we focused on several mediators such as Bcl2, Bcl Xl, and Mcl1, regulating Ca^{2+} transfer from ER to mitochondria by suppressing IP3R [28]. Western blot analysis revealed that only Bcl2 and Bcl XL were significantly differentially expressed among the groups, and the trend was consistent with the level of Bmal1 (Fig. 7A, C and Suppl. Fig. 4B). The outcomes of CoIP analysis demonstrated that the protein interaction between Bcl2 and IP3R was significantly inhibited in CON-Ad-shBmal1 and HGHP-Ad-Ctrl cells, and this was rescued by Bmal1 overexpression (Fig. 7D and E). However, we did not observe the binding of Bcl XL to IP3R (Fig. 7D).

Bmal1 is a core circadian transcription factor that modulates the downstream genes through coupling with the E-box elements in their promoters [15]. Thus, we performed the ChIP assay, which revealed a significant decline in the interaction between Bmal1 and the promoter region of Bcl2 following HGHP treatment. As expected, vector-mediated Bmal1 overexpression enhanced this binding in H9c2 cells (Fig. 7F). As a positive reference, the Per1 DNA fragment precipitated by Bmal1 antibody was also examined. We then examined the rhythmicity of Bcl2 in T2D mice hearts (Fig. 7G–I). Compared with CON, rhythmicity and oscillation of Bcl2 mRNA (Fig. 7G) and protein (Fig. 7H and I) were all significantly attenuated at all ZT points in T2D mice hearts, which were consistent with Bmal1 changes (Fig. 1A, C, D). The canonical E-box sequences (CANNTG) in the *Per1* and *Bcl2* gene promoter regions and primer sequences utilized for qPCR are presented in Supplementary Table 2.

3.7. BIRD-2 aggravates mitochondrial Ca^{2+} overload and apoptosis in HGHP-induced H9c2 cardiomyoblasts

BIRD-2, a peptide that specifically disrupts the Bcl2/IP3R complex, was utilized to further verify the mitochondrial Ca^{2+} regulatory mechanism via the Bmal1-Bcl2/IP3R signaling pathway. As shown in Fig. 8A–C, the treatment of BIRD-2 blocked the binding of Bcl2 and IP3R, and led to upregulation in the c-Caspase3 in HGHP-treated cells with or without high expression of Bmal1. Moreover, in H9c2 cells co-treated with BIRD-2 and HGHP, the mitochondrial Ca^{2+} levels were significantly increased regardless of Bmal1 overexpression (Fig. 8D and E). Accordingly, contrasted to the respective control group, MDA and 4-hydroxynonena (4-HNE) levels in HGHP-Ad-Ctrl-BIRD and HGHP-Ad-Bmal1-BIRD cells were also significantly increased (Fig. 8F and G). Similarly, mitochondrial ROS levels were higher within cells supplemented with BIRD-2 contrasted to those incubated via HGHP or in the Ad-Bmal1 transfected group (Fig. 8H and I). Collectively, these data suggested that inhibition of Bmal1 prevented the Bcl2/IP3R binding, which enhanced Ca^{2+} transport via IP3R in MAMs, leading to mitochondrial Ca^{2+} overload and apoptosis.

4. Discussion

This is the first study to discover the underlying molecular mechanism of Bmal1 in diabetic myocardial injury. The novel findings were as follows: Firstly, the rhythmicity and oscillation of the Bmal1 gene were significantly weakened in whether *in vivo* or *in vitro* models of DCM. Secondly, Bmal1 downregulation caused myocardial injury by aggravating mitochondrial damages and subsequent apoptosis, possibly due to excess mitochondrial ROS and Ca^{2+} overload. Thirdly, Bmal1 downregulation decreased the transcription of Bcl2, thus weakening the interaction with IP3R and enhancing Ca^{2+} transfer in MAMs, which may lead to mitochondrial Ca^{2+} overload. Importantly, restoring Bmal1 expression effectively alleviated mitochondrial Ca^{2+} overload and apoptosis and consequently improved myocardial injuries. Therefore, maintaining circadian rhythm homeostasis, especially targeting the regulation of Bmal1, is crucial for DCM treatment.

DCM is a condition that arises due to prolonged diabetes, leading to alterations in the composition and role of the myocardium, resulting in heart failure [1,4,30]. Herein, heart tissues from diabetic patients and animal models showed that mitochondrial dysfunction promotes DCM development. Many mechanisms causing mitochondrial damage in the heart simultaneously activate signaling pathways that promote apoptosis [3–5]. In the present study, mitochondrial injuries and increased apoptosis were observed in T2D mice, which were characterized by cardiac hypertrophy and diastolic dysfunction. Circadian clock machinery orchestrates internal daily rhythms of molecular and cellular mechanisms, resulting in circadian differences within physiology and behaviors [15,31]. Daily variation of glucose tolerance and insulin sensitivity is one of the most pronounced circadian rhythms in humans. Importantly, disruption of circadian oscillations in glucose metabolism is a hallmark of T2D [32]. Rhythmic expressions of clock genes are decreased in peripheral leucocytes, liver, renal and adipose tissue of T2D models [33–35]. Although the disturbances of the molecular clock within T2D might be due to insulin resistance or obesity-related factors, like leptin disorder [34,36], this does not explain Bmal1 downregulation in T1D [37]. A study showed that dysfunction of AMPK and SIRT1 in obese mice may downregulate Bmal1 in white adipose tissue [38]. In this study, the mechanism of decreased myocardial Bmal1 expression in DCM was not elucidated and thus will serve as the primary focus of our upcoming works.

Moreover, further studies should assess whether the downregulation of Bmal1 is involved in DCM development. DCM-like changes in CKB mice were reversed by heart-specific overexpression of Bmal1, indicating that Bmal1 performs a critical function in DCM pathogenesis. The intrinsic mitochondrial apoptotic pathway has a vital role in cell survival

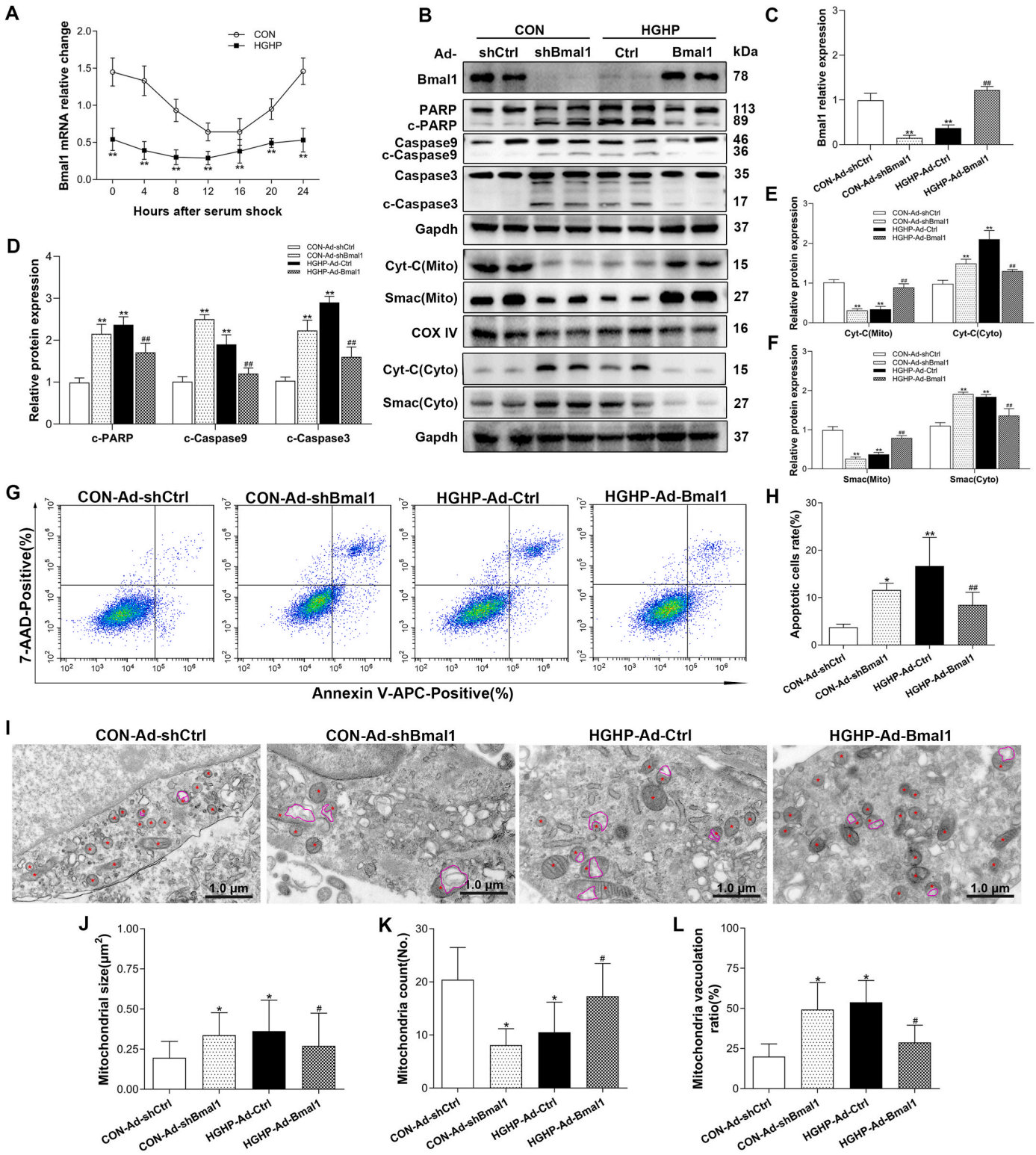

Fig. 4. Inhibition of Bmal1 aggravated mitochondrial damage and apoptosis *in vitro*. (A) Bmal1 mRNA levels under HGHP conditions at different time after serum shock. (B) Western blots showing expression level of Bmal1 and apoptotic proteins associated with the intrinsic mitochondrial pathway. (C, D) Quantification of Bmal1, c-PARP and c-Caspase9/3 protein levels in whole cell lysates. Presenting as fold changes relative to the CON-Ad-shCtrl group. (E, F) Quantification of Cyt-C and Smac protein levels in mitochondria lysates or cytosol lysates. Presenting as fold changes relative to the CON-Ad-shCtrl group. (G, H) Cell apoptosis rate was determined using flow cytometry. (I) Representative TEM images of mitochondria in H9c2 cardiomyoblasts under different treatments. Scale bar: 1 μm. Red asterisk, mitochondria; purple circle, vacuole. (J–L) Statistical analysis of mitochondrial size, count and vacuolation. Total 60 mitochondria were calculated per group. Each experiment was repeated three times. Data are presented as the mean ± SD. Statistical significance was determined using two-way repeated measures ANOVA (A) or two-way ANOVA (C–F, H, J-L) with Bonferroni post-hoc tests. $^{*}P < 0.05$ and $^{**}P < 0.01$ vs. CON-Ad-shCtrl. $^{\#}P < 0.05$ and $^{\#\#}P < 0.01$ vs. HGHP-Ad-Ctrl.

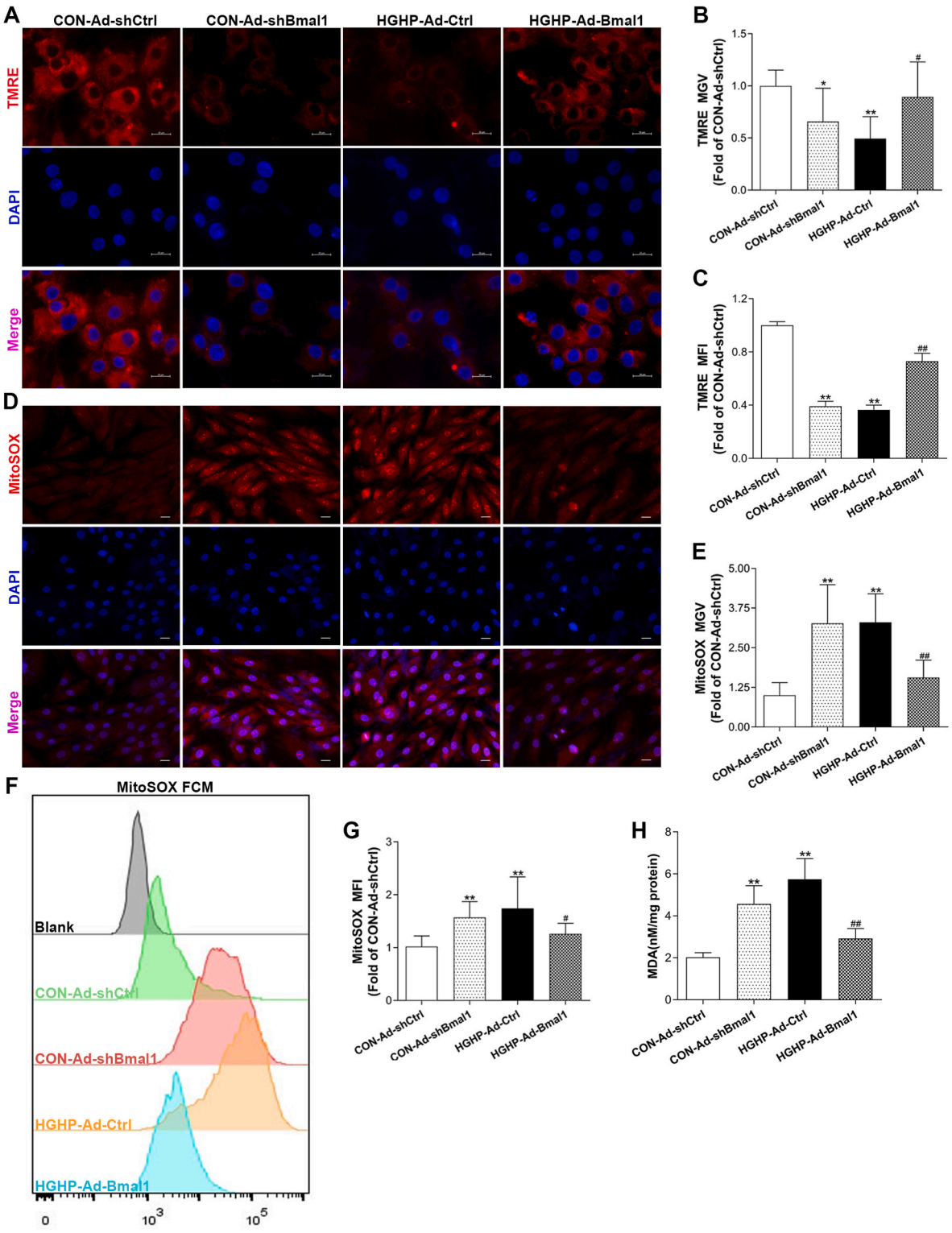

Fig. 5. Determination of mitochondrial membrane potential and ROS accumulation in cultured H9c2 cells. (A, B) Mitochondrial membrane potential labeled by TMRE was detected under a fluorescence microscope and quantification of relative MGV of TMRE. Scale bar: 20 μm. (C) MFI detection of TMRE using a fluorescence microplate reader. (D, E) Mitochondria ROS marked by MitoSOX probe was measured using fluorescence microscope and quantification of relative MGV of MitoSOX. Scale bar: 10 μm. (F, G) Mitochondria ROS marked by MitoSOX probe was measured using flow cytometry and MFI quantification of MitoSOX. (H) MDA levels in whole cell lysates. Each experiment was repeated three times. Data are presented as the mean ± SD. Statistical significance was determined using two-way ANOVA with Bonferroni post-hoc tests. $^{*}P < 0.05$ and $^{**}P < 0.01$ vs. CON-Ad-shCtrl. $^{\#}P < 0.05$ and $^{\#\#}P < 0.01$ vs. HGHP-Ad-Ctrl.

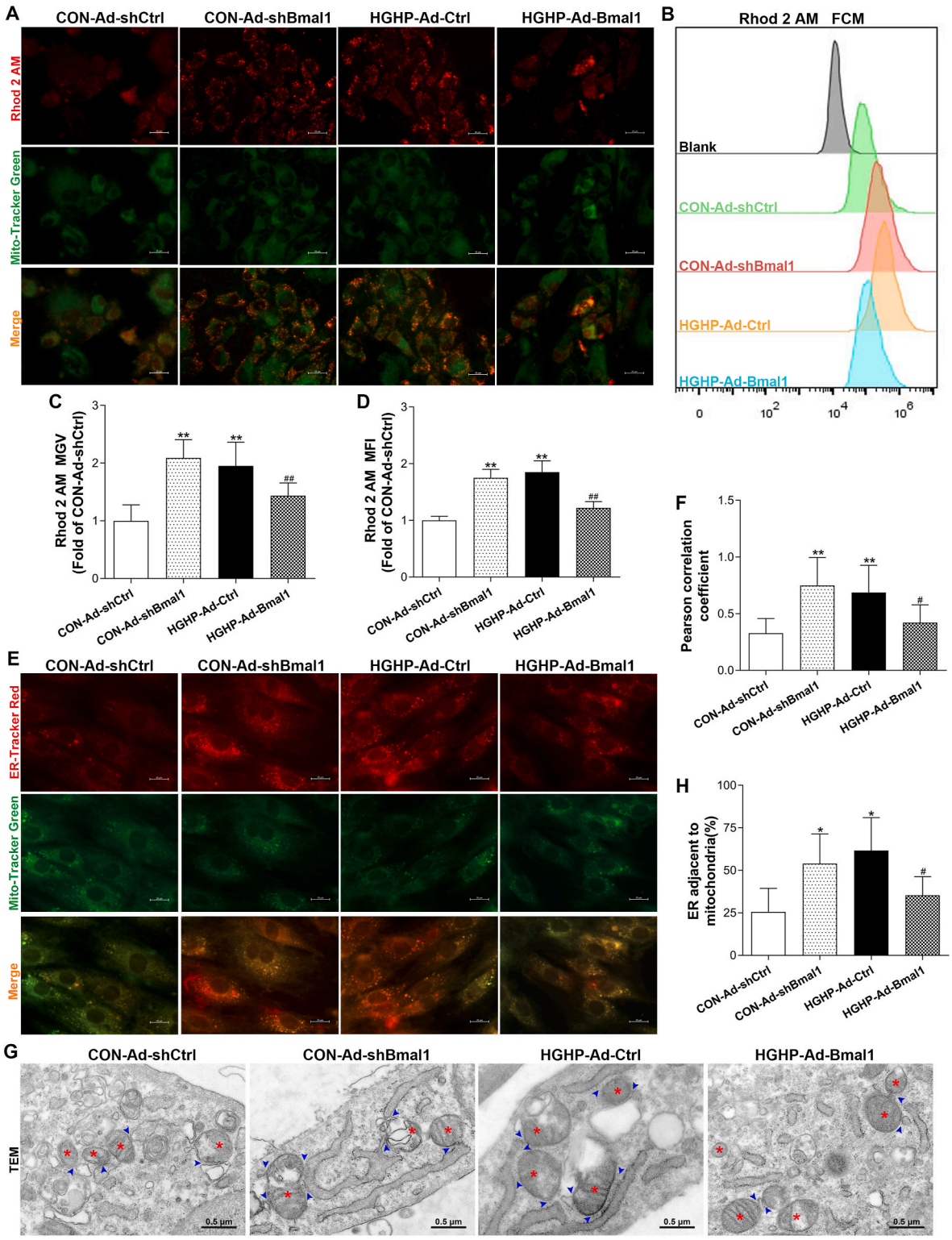

Fig. 6. Impact of Bmal1 expression on MAMs formation and mitochondrial Ca^{2+} content *in vitro*. (A) Rhod 2 a.m. and Mito Tracker Green co-staining to determine mitochondrial Ca^{2+} content. Scale bar: 20 μm. (B) Flow cytometry results showing the fluorescence intensity of Rhod 2 a.m. (C) Quantification of relative MGV of the Rhod-2 AM/MitoTracker Green-dual positive areas in fluorescence images. (D) Quantitative Rhod 2 a.m. MFI detected by flow cytometry. (E, F) ER-Tracker Red and Mito-Tracker Green co-labelling to observe MAMs. Scale bar: 20 μm. Pearson correlation coefficient was calculated. (G, H) TEM images of mitochondria and ER proximity in H9c2 cells. Scale bar: 0.5 μm. Red asterisk, mitochondria; blue triangle, ER adjacent to mitochondria contacts. Each experiment was repeated three times. Data are presented as the mean ± SD. Statistical significance was determined using two-way ANOVA with Bonferroni post-hoc tests. $^{*}P < 0.05$ and $^{**}P < 0.01$ vs. CON-Ad-shCtrl. $^{\#}P < 0.05$ and $^{\#\#}P < 0.01$ vs. HGHP-Ad-Ctrl.

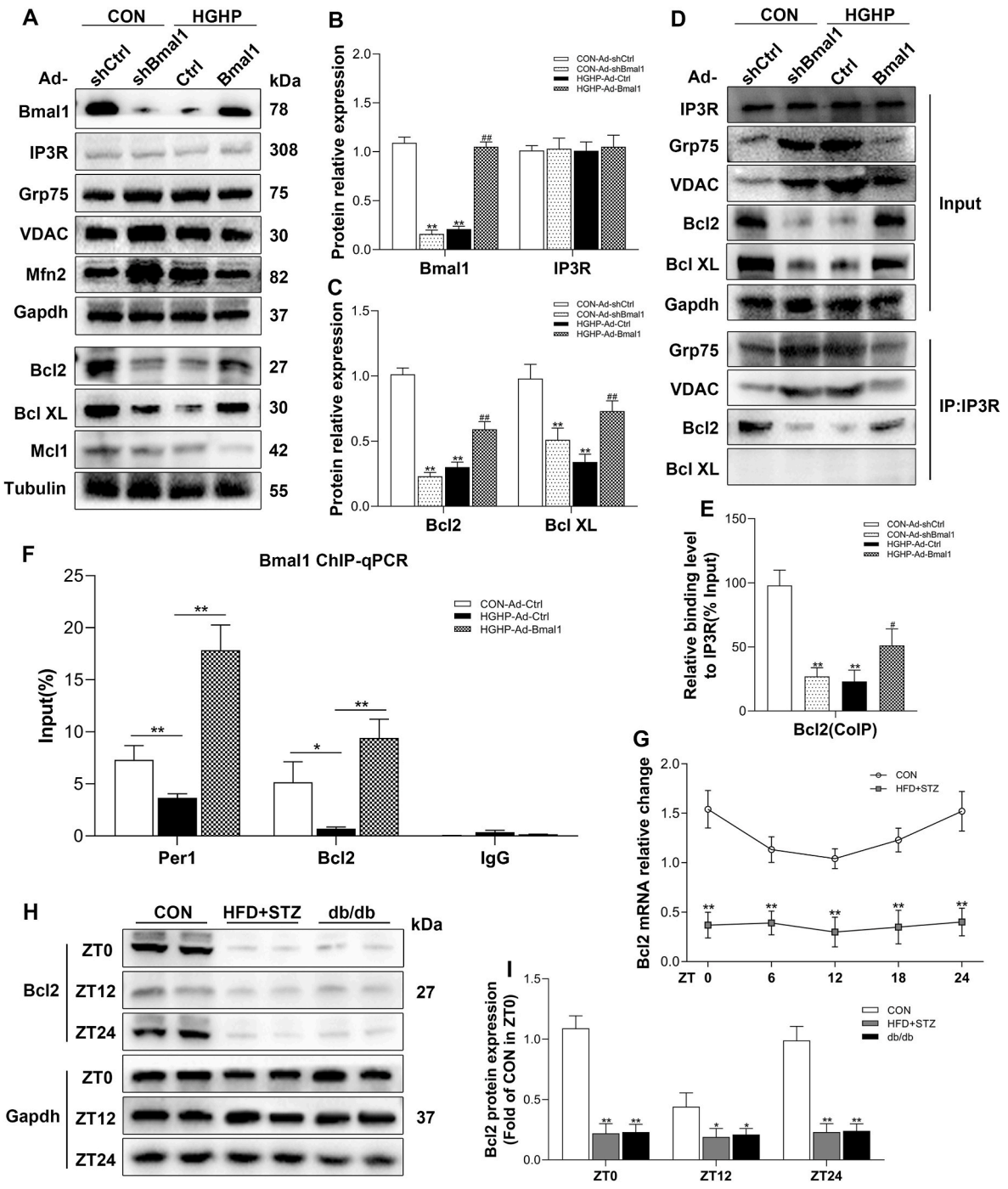

Fig. 7. Downregulation of Bmal1 relieved the inhibitory effect of Bcl2 on IP3R. (A) Western blots showing expression level of proteins in MAMs (IP3R, Grp75, VDAC, and Mfn2) and anti-apoptotic proteins (Bcl2, Bcl XL and Mcl1). (B, C) Quantification of Bmal1, IP3R, Bcl2 and Bcl XL protein levels. Presenting as fold changes relative to the CON-Ad-shCtrl group. $^{**}P < 0.01$ vs. CON-Ad-shCtrl. $^{\#\#}P < 0.01$ vs. HGHP-Ad-Ctrl. (D) Verification of the proteins that interact with IP3R through CoIP assays. (E) Quantification of binding level of Bcl2 to IP3R in input. Presenting as fold changes relative to the CON-Ad-shCtrl group (%). $^{**}P < 0.01$ vs. CON-Ad-shCtrl. $^{\#}P < 0.05$ vs. HGHP-Ad-Ctrl. (F) ChIP-qPCR analysis of the Bmal1 binding to promoter regions of *Per1* and *Bcl2* genes. * denotes $P < 0.05$ and ** denotes $P < 0.01$. (G) Bcl2 mRNA levels at different ZT points (ZT0-24). n = 3 mice per group per ZT point. $^{**}P < 0.01$ vs. CON. (H, I) Protein expression levels of Bcl2 at ZT0, ZT12 and ZT24 as determined by Western blots. n = 3 mice per group per ZT point. $^{**}P < 0.01$ vs. CON. If not specifically stated, each experiment was repeated three times. Data are presented as the mean ± SD. Statistical significance was determined using two-way ANOVA (B, C, E), one-way ANOVA (F) or two-way repeated measures ANOVA (G, I) with Bonferroni post-hoc tests.

and also triggers DCM [39,40]. In this study, Bmal1 overexpression relieved mitochondrial injuries and apoptosis *in vivo* and *in vitro*, indicating that Bmal1 deficiency participates in DCM development through mitochondria-mediated apoptosis. Abnormal mitochondria are a major generator of ROS, which can induce the opening of mPTP, releasing Cyto C and Smac, and then cause caspase 9 to activate caspase 3[40]. In our study, overexpressing Bmal1 in a diabetic heart could relieve the overproduction of ROS remarkably, although the ROS levels remained high in T2D + AAV-Bmal1 groups (Fig. 3H and I). Earlier studies showed that inhibition of Bmal1 activates Leydig cell apoptosis [41] and accelerates atherosclerotic progression [42]. Although these studies explored the relationship between Bmal1 and apoptosis, the potential mediating role

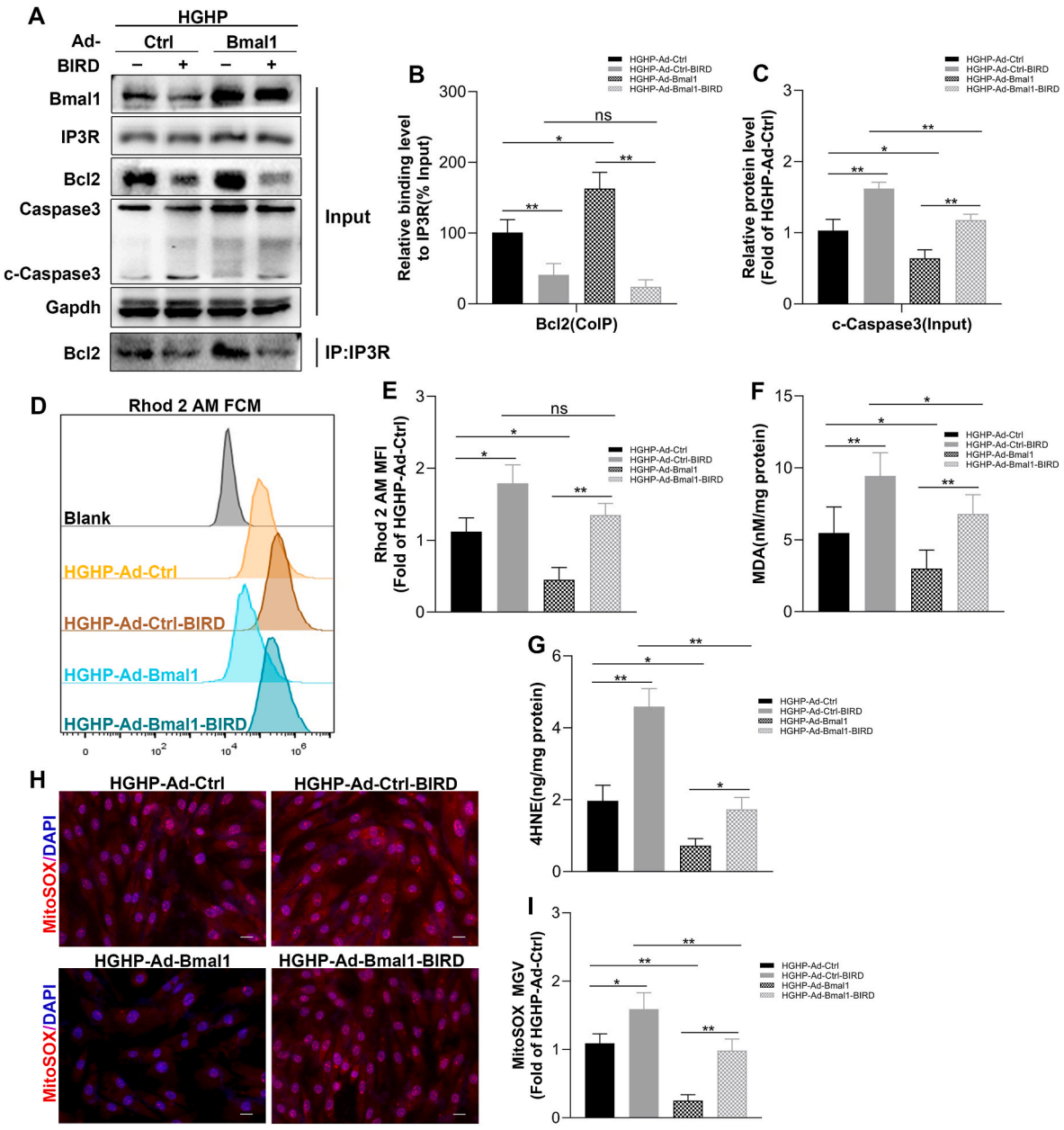

Fig. 8. BIRD-2 aggravated mitochondrial Ca^{2+} overload and apoptosis *in vitro*. (A) Bcl2 binding level to IP3R and c-Caspase3 level were detected by immunoblotting and immunoprecipitation after treatment with control or BIRD-2 peptides. (B) Quantification of Bcl2 binding level to IP3R in input Presenting as fold changes relative to the HGHP-Ad-shCtrl group (%). (C) Quantification of c-Caspase3 level in input. Presenting as fold changes relative to the HGHP-Ad-shCtrl group. (D, E) Measurement of mitochondrial Ca^{2+} levels by flow cytometry and quantification of Rhod 2 a.m. MFI. (F, G) MDA and 4-HNE levels in whole cell lysates. (H) MitoSOX fluorescence staining showing the mitochondrial ROS levels. Scale bar: 10 μm. (I) Quantification of MitoSOX MGV. Each experiment was repeated three times. Data are presented as the mean ± SD. Statistical significance was determined using two-way ANOVA with Bonferroni post-hoc tests. * denotes $P < 0.05$, ** denotes $P < 0.01$ and ns denotes no significance.

of mitochondria is unclear. Recently, a study showed that Bmal1-mediated autophagy exerts a protective part in a diabetic myocardial ischemia/reperfusion rat model [43]. Another study also demonstrated the regulatory role of Bmal1 on autophagy through the mTOR signaling pathway in neonatal rats cardiomyocytes [44]. In this work, defective autophagy and cardiomyocyte injury induced by high glucose were improved by Bmal1 overexpression and aggravated by its knockdown [44]. According to our best understanding, this is the first investigation to reveal that disruption of Bmal1 results in intrinsic mitochondria-mediated activation of apoptosis in DCM.

Mitochondrial Ca^{2+} homeostasis is involved in different physiological and pathological cell processes, such as energy metabolism, apoptosis, and ROS production [9]. MAMs, where ER and mitochondrial membranes are in similar proximity, create distinct contact sites for ER/mitochondria Ca^{2+} signaling [11]. Ca^{2+} transfer through MAMs regulates mitochondrial function and stimulus for the intrinsic apoptosis pathway in cardiac myocytes [9,24,45]. In the present study, Bmal1 downregulation was strongly associated with enhanced MAMs formation and mitochondrial Ca^{2+} overload. Clock genes are essential regulators for circadian cytosolic Ca^{2+} rhythms in SCN neurons [46,47]. Nevertheless, the relationship between Bmal1 and cytosolic or mitochondrial Ca^{2+} in DCM is unclear. In this work, results showed that Bmal1 was associated with MAMs-related mitochondrial Ca^{2+} overload in cardiomyocytes in diabetic mice. Although MAMs formation was

increased, IP3R expression was not significantly changed, which could not fully elucidate mitochondrial Ca^{2+} overload. Since IP3R is the main channel protein responsible for Ca^{2+} transport in MAMs, then we focused on the activity of IP3R. Bcl-2 controls intrinsic mitochondrial apoptosis and mitochondrial dynamics [48] and can target IP3R and inhibit its activity, thereby blocking Ca^{2+}-dependent apoptosis [28,49]. Herein, Bmal1 downregulation decreased the binding between IP3R and Bcl2. However, Bmal1 overexpression *in vitro* restored this interaction. Furthermore, ChIP-qPCR confirmed that Bmal1 can bind directly to the Bcl2 gene promoter region, thereby playing a transcriptional regulatory role. Bcl2 is comprised of four distinct Bcl-2 homology (BH) domains, of which BH4 is mainly correlated with coupling to IP3R [28,49]. BIRD-2 peptide exhibits competitive binding properties towards the BH4 domain of Bcl2 to disrupt the Bcl2/IP3R complex, thereby relieving the inhibition of IP3R [28,49,50]. In the present study, additional BIRD-2 aggravated mitochondrial Ca^{2+} overload and apoptotic phenotype. However, Bmal1 overexpression in HGHP conditions improved mitochondrial Ca^{2+} overload and apoptotic phenotype. These findings indicate that Bmal1 insufficiency can impede the interaction between Bcl2 and IP3R at their central domains.

Previous studies have also shown that CKB mice can develop age-related dilated cardiomyopathy with decreased systolic function [51,52], inconsistent with the echocardiographic results obtained from CKB mice at 31 weeks of age (24 weeks post tamoxifen injection). Mellani et al. detected enlarged hearts and reduced mean cardiomyocytes in Bmal1 knockout mice germline at four weeks of age, suggesting that Bmal1 deficiency can cause cardiomyocyte hyperplasia [53]. In our study, the knockout of Bmal1 gene in CKB mice was induced via intraperitoneal injection of tamoxifen at the age of 8 weeks, when the hearts were fully developed. Therefore, the age of mice at the time of Bmal1 knockout may be critical for the emergence of different phenotypes.

5. Conclusion

In summary, decreased expression of the circadian gene Bmal1 decreases Bcl2 transcription and weakens Bcl2/IP3R interaction, thus promoting IP3R activity and Ca^{2+} release from ER to mitochondria, ultimately activating mitochondria-mediated apoptosis and promoting DCM development. This study shows that targeting cardiomyocyte Bmal1 may be promising for the treatment of DCM in the future.

Author contributions

JGZ designed and coordinated the study. NNZ and HY conducted and analyzed the majority of the investigation, and NNZ drafted the manuscript. TZL, ZHZ, and BF performed and analyzed partial cell experiment data (mitochondrial function measurements). YW, ZYQ, and XFH analyzed and inspected the study. All authors have reviewed and approved the submitted manuscript.

Funding

This work was funded from the National Natural Science Foundation of China (81870251, 82100374) and Suzhou Science and Technology Fund (SYS2020103).

Declaration of competing interest

The authors declare that they have no known competing financial interests or personal relationships that could have appeared to influence the work reported in this paper.

Data availability

Data will be made available on request.

Acknowledgments

We thank Dr. Jiateng Sun and Prof. Meijuan Zou for helpful discussions and comments on the manuscript and for generously sharing their reagents.

Appendix A. Supplementary data

Supplementary data to this article can be found online at https://doi.org/10.1016/j.redox.2023.102788.

Abbreviations

T2D	Type 2 diabetes
HF	heart failure
DCM	diabetic cardiomyopathy
ROS	reactive oxygen species
MMP	mitochondrial membrane potential
mPTP	mitochondrial permeability transition pore
ER	endoplasmic reticulum
MAMs	mitochondria-associated ER membranes
TTFLs	transcription-translation feedback loops
ZT	zeitgeber time
IPGTT	intraperitoneal glucose tolerance test
ANP	atrial natriuretic peptide
BNP	brain natriuretic peptid
WGA	wheat germ agglutinin
TUNEL	terminal deoxynucleotidyl transferase-mediated dUTP in situ nick end labelling
PWD	pulse wave doppler
MFI	mean fluorescence intensity
MGV	mean grey value
IVST	interventricular septal wall thickness
CSA	cross section area
BW	body weight
HW	heart weight
TL	tibia length
HR	heart rate
LV	left ventricular
LVESD	LV end systolic dimension
LVEDD	LV end diastolic dimension
LVAWs/d	LV anterior wall in systole/diastole
LVPWs/d	IVRT, iso-volumetric relaxation time
LV MPI	LV myocardial performance index
LVFS	LV fractional shortening
LVEF	LV ejection fraction
CO	cardiac output
BIRD-2	Bcl/IP3R disruptor-2

References

[1] S. Rubler, J. Dlugash, Y.Z. Yuceoglu, T. Kumral, A.W. Branwood, A. Grishman, New type of cardiomyopathy associated with diabetic glomerulosclerosis, Am. J. Cardiol. 30 (1972) 595–602.
[2] J.B. Echouffo-Tcheugui, S. Zhang, R. Florido, C. Hamo, J.S. Pankow, E.D. Michos, R.B. Goldberg, V. Nambi, G. Gerstenblith, W.S. Post, R.S. Blumenthal, C. M. Ballantyne, J. Coresh, E. Selvin, C.E. Ndumele, Duration of diabetes and incident heart failure, JACC (J. Am. Coll. Cardiol.): Heart Fail. 9 (2021) 594–603.
[3] R.H. Ritchie, E.D. Abel, Basic mechanisms of diabetic heart disease, Circ. Res. 126 (2020) 1501–1525.
[4] W.H. Dillmann, Diabetic cardiomyopathy, Circ. Res. 124 (2019) 1160–1162.
[5] G. Jia, M.A. Hill, J.R. Sowers, Diabetic cardiomyopathy: an update of mechanisms contributing to this clinical entity, Circ. Res. 122 (2018) 624–638.
[6] B. Zhou, R. Tian, Mitochondrial dysfunction in pathophysiology of heart failure, J. Clin. Invest. 128 (2018) 3716–3726.
[7] Z. Qiu, Y. Wei, Q. Song, B. Du, H. Wang, Y. Chu, Y. Hu, The role of myocardial mitochondrial quality control in heart failure, Front. Pharmacol. 10 (2019) 1404.
[8] X. Chang, Y. Li, C. Cai, F. Wu, J. He, Y. Zhang, J. Zhong, Y. Tan, R. Liu, H. Zhu, H. Zhou, Mitochondrial quality control mechanisms as molecular targets in diabetic heart, Metab. Clin. Exp. 137 (2022), 155313.

[9] D. Zhang, F. Wang, P. Li, Y. Gao, Mitochondrial Ca2+ homeostasis: emerging roles and clinical significance in cardiac remodeling, Int. J. Mol. Sci. 23 (2022) 3025.
[10] G. Murtaza, H.U.H. Virk, M. Khalid, C.J. Lavie, H. Ventura, D. Mukherjee, V. Ramu, S. Bhogal, G. Kumar, M. Shanmugasundaram, T.K. Paul, Diabetic cardiomyopathy - a comprehensive updated review, Prog. Cardiovasc. Dis. 62 (2019) 315–326.
[11] Y. Chen, Y. Xin, Y. Cheng, X. Liu, Mitochondria-endoplasmic reticulum contacts: the promising regulators in diabetic cardiomyopathy, Oxid. Med. Cell. Longev. (2022), 2531458, 2022.
[12] J.H. Ma, S. Shen, J.J. Wang, Z. He, A. Poon, J. Li, J. Qu, S.X. Zhang, Comparative proteomic analysis of the mitochondria-associated ER membrane (MAM) in a long-term type 2 diabetic rodent model, Sci. Rep. 7 (2017), 2062-2062.
[13] L.P. Shearman, S. Sriram, D.R. Weaver, E.S. Maywood, I. Chaves, B. Zheng, K. Kume, C.C. Lee, G.T. van der Horst, M.H. Hastings, S.M. Reppert, Interacting molecular loops in the mammalian circadian clock, Science 288 (2000) 1013–1019.
[14] J.C. Dunlap, Molecular bases for circadian clocks, Cell 96 (1999) 271–290.
[15] N. Koike, S.H. Yoo, H.C. Huang, V. Kumar, C. Lee, T.K. Kim, J.S. Takahashi, Transcriptional architecture and chromatin landscape of the core circadian clock in mammals, Science 338 (2012) 349–354.
[16] D. Whitmore, N.S. Foulkes, P. Sassone-Corsi, Light acts directly on organs and cells in culture to set the vertebrate circadian clock, Nature 404 (2000) 87–91.
[17] C. Jouffe, B.D. Weger, E. Martin, F. Atger, M. Weger, C. Gobet, D. Ramnath, A. Charpagne, D. Morin-Rivron, E.E. Powell, M.J. Sweet, M. Masoodi, N. H. Uhlenhaut, F. Gachon, Disruption of the circadian clock component BMAL1 elicits an endocrine adaption impacting on insulin sensitivity and liver disease, Proc. Natl. Acad. Sci. U. S. A. 119 (2022), e2200083119.
[18] B.M. Gabriel, A. Altıntaş, J.A.B. Smith, L. Sardon-Puig, X. Zhang, A.L. Basse, R. C. Laker, H. Gao, Z. Liu, L. Dollet, J.T. Treebak, A. Zorzano, Z. Huo, M. Rydén, J. T. Lanner, K.A. Esser, R. Barrès, N.J. Pillon, A. Krook, J.R. Zierath, Disrupted circadian oscillations in type 2 diabetes are linked to altered rhythmic mitochondrial metabolism in skeletal muscle, Sci. Adv. 7 (2021), eabi9654.
[19] G.R. McGinnis, Y. Tang, R.A. Brewer, M.K. Brahma, H.L. Stanley, G. Shanmugam, N.S. Rajasekaran, G.C. Rowe, S.J. Frank, A.R. Wende, E.D. Abel, H. Taegtmeyer, S. Litovsky, V. Darley-Usmar, J. Zhang, J.C. Chatham, M.E. Young, Genetic disruption of the cardiomyocyte circadian clock differentially influences insulin-mediated processes in the heart, J. Mol. Cell. Cardiol. 110 (2017) 80–95.
[20] B. Lieberman, T.A. Martino, L.A. Kirshenbaum, Circadian-regulated cell death in cardiovascular diseases, Circulation 139 (2019) 965–980.
[21] T. Pan, J. Liu, S. Xu, Q. Yu, H. Wang, H. Sun, J. Wu, Y. Zhu, J. Zhou, Y. Zhu, ANKRD22, a novel tumor microenvironment-induced mitochondrial protein promotes metabolic reprogramming of colorectal cancer cells, Theranostics 10 (2020) 516–536.
[22] K. Srinivasan, B. Viswanad, L. Asrat, C.L. Kaul, P. Ramarao, Combination of high-fat diet-fed and low-dose streptozotocin-treated rat: a model for type 2 diabetes and pharmacological screening, Pharmacol. Res. 52 (2005) 313–320.
[23] A. Balsalobre, F. Damiola, U. Schibler, A serum shock induces circadian gene expression in mammalian tissue culture cells, Cell 93 (1998) 929–937.
[24] H.X. Xu, S.M. Cui, Y.M. Zhang, J. Ren, Mitochondrial Ca(2+) regulation in the etiology of heart failure: physiological and pathophysiological implications, Acta Pharmacol. Sin. 41 (2020) 1301–1309.
[25] S. Wu, Q. Lu, Y. Ding, Y. Wu, Y. Qiu, P. Wang, X. Mao, K. Huang, Z. Xie, M.-H. Zou, Hyperglycemia-driven inhibition of AMP-activated protein kinase α2 induces diabetic cardiomyopathy by promoting mitochondria-associated endoplasmic reticulum membranes in vivo, Circulation 139 (2019) 1913–1936.
[26] R.I. Fonteriz, S. de la Fuente, A. Moreno, C.D. Lobatón, M. Montero, J. Alvarez, Monitoring mitochondrial [Ca2+] dynamics with rhod-2, ratiometric pericam and aequorin, Cell Calcium 48 (2010) 61–69.
[27] M. Federico, M. Zavala, T. Vico, S. López, E. Portiansky, S. Alvarez, M.C.V. Abrille, J. Palomeque, CaMKII activation in early diabetic hearts induces altered sarcoplasmic reticulum-mitochondria signaling, Sci. Rep. 11 (2021), 20025.
[28] I. Dulloo, P. Atakpa-Adaji, Y.-C. Yeh, C. Levet, S. Muliyil, F. Lu, C.W. Taylor, M. Freeman, iRhom pseudoproteases regulate ER stress-induced cell death through IP3 receptors and BCL-2, Nat. Commun. 13 (2022) 1257.
[29] A. Bartok, D. Weaver, T. Golenár, Z. Nichtova, M. Katona, S. Bánsághi, K. J. Alzayady, V.K. Thomas, H. Ando, K. Mikoshiba, S.K. Joseph, D.I. Yule, G. Csordás, G. Hajnóczky, IP(3) receptor isoforms differently regulate ER-mitochondrial contacts and local calcium transfer, Nat. Commun. 10 (2019) 3726.
[30] C. Cai, F. Wu, J. He, Y. Zhang, N. Shi, X. Peng, Q. Ou, Z. Li, X. Jiang, J. Zhong, Y. Tan, Mitochondrial quality control in diabetic cardiomyopathy: from molecular mechanisms to therapeutic strategies, Int. J. Biol. Sci. 18 (2022) 5276–5290.
[31] S.M. Reppert, D.R. Weaver, Coordination of circadian timing in mammals, Nature 418 (2002) 935–941.
[32] K. Ijiri, C.S. Potten, Circadian rhythms in the incidence of apoptotic cells and number of clonogenic cells in intestinal crypts after radiation using normal and reversed light conditions, Int. J. Radiat. Biol. Relat. Stud. Phys. Chem. Med. 53 (1988) 717–727.
[33] H. Ando, T. Takamura, N. Matsuzawa-Nagata, K.R. Shima, T. Eto, H. Misu, M. Shiramoto, T. Tsuru, S. Irie, A. Fujimura, S. Kaneko, Clock gene expression in peripheral leucocytes of patients with type 2 diabetes, Diabetologia 52 (2009) 329–335.
[34] H. Ando, M. Kumazaki, Y. Motosugi, K. Ushijima, T. Maekawa, E. Ishikawa, A. Fujimura, Impairment of peripheral circadian clocks precedes metabolic abnormalities in ob/ob mice, Endocrinology 152 (2011) 1347–1354.
[35] Q. Luo, Y. Xiao, A. Alex, T.R. Cummins, A.D. Bhatwadekar, The diurnal rhythm of insulin receptor substrate-1 (IRS-1) and Kir4.1 in diabetes: implications for a clock gene Bmal1, Invest. Ophthalmol. Vis. Sci. 60 (2019) 1928–1936.
[36] K. Honma, M. Hikosaka, K. Mochizuki, T. Goda, Loss of circadian rhythm of circulating insulin concentration induced by high-fat diet intake is associated with disrupted rhythmic expression of circadian clock genes in the liver, Metab. Clin. Exp. 65 (2016) 482–491.
[37] Z. Qiu, H. Ming, S. Lei, B. Zhou, B. Zhao, Y. Yu, R. Xue, Z. Xia, Roles of HDAC3-orchestrated circadian clock gene oscillations in diabetic rats following myocardial ischaemia/reperfusion injury, Cell Death Dis. 12 (2021), 43-43.
[38] P.W. Caton, J. Kieswich, M.M. Yaqoob, M.J. Holness, M.C. Sugden, Metformin opposes impaired AMPK and SIRT1 function and deleterious changes in core clock protein expression in white adipose tissue of genetically-obese db/db mice, Diabetes Obes. Metabol. 13 (2011) 1097–1104.
[39] F.J. Bock, S.W.G. Tait, Mitochondria as multifaceted regulators of cell death, Nat. Rev. Mol. Cell Biol. 21 (2020) 85–100.
[40] J. Wei, Y. Zhao, H. Liang, W. Du, L. Wang, Preliminary evidence for the presence of multiple forms of cell death in diabetes cardiomyopathy, Acta Pharm. Sin. B 12 (2022) 1–17.
[41] H. Ding, J. Zhao, H. Liu, J. Wang, W. Lu, BMAL1 knockdown promoted apoptosis and reduced testosterone secretion in TM3 Leydig cell line, Gene 747 (2020), 144672.
[42] M. Xie, Q. Tang, J. Nie, C. Zhang, X. Zhou, S. Yu, J. Sun, X. Cheng, N. Dong, Y. Hu, L. Chen, BMAL1-Downregulation aggravates porphyromonas gingivalis-induced atherosclerosis by encouraging oxidative stress, Circ. Res. 126 (2020) e15–e29.
[43] Z. Qiu, H. Ming, Y. Zhang, Y. Yu, S. Lei, Z-y Xia, The protective role of bmal1-regulated autophagy mediated by HDAC3/SIRT1 pathway in myocardial ischemia/reperfusion injury of diabetic rats, Cardiovasc. Drugs Ther. 2 (2022) 229–243.
[44] L. Qiao, B. Guo, H. Zhang, R. Yang, L. Chang, Y. Wang, X. Jin, S. Liu, Y. Li, The clock gene, brain and muscle Arnt-like 1, regulates autophagy in high glucose-induced cardiomyocyte injury, Oncotarget 8 (2017) 80612–80624.
[45] G.L. Smith, D.A. Eisner, Calcium buffering in the heart in health and disease, Circulation 139 (2019) 2358–2371.
[46] M. Ikeda, M. Ikeda, Bmal1 is an essential regulator for circadian cytosolic Ca^{2+} rhythms in suprachiasmatic nucleus neurons, J. Neurosci. : the official journal of the Society for Neuroscience 34 (2014) 12029–12038.
[47] T. Noguchi, T.L. Leise, N.J. Kingsbury, T. Diemer, L.L. Wang, M.A. Henson, D. K. Welsh, Calcium circadian rhythmicity in the suprachiasmatic nucleus: cell autonomy and network modulation, eNeuro 4 (4) (2017).
[48] H. Ivanova, L.E. Wagner 2nd, A. Tanimura, E. Vandermarliere, T. Luyten, K. Welkenhuyzen, K.J. Alzayady, L. Wang, K. Hamada, K. Mikoshiba, H. De Smedt, L. Martens, D.I. Yule, J.B. Parys, G. Bultynck, Bcl-2 and IP(3) compete for the ligand-binding domain of IP(3)Rs modulating Ca(2+) signaling output, Cell. Mol. Life Sci. : CM 76 (2019) 3843–3859.
[49] N. Rosa, H. Ivanova, L.E. Wagner 2nd, J. Kale, R. La Rovere, K. Welkenhuyzen, N. Louros, S. Karamanou, V. Shabardina, I. Lemmens, E. Vandermarliere, K. Hamada, H. Ando, F. Rousseau, J. Schymkowitz, J. Tavernier, K. Mikoshiba, A. Economou, D.W. Andrews, J.B. Parys, D.I. Yule, G. Bultynck, Bcl-xL acts as an inhibitor of IP(3)R channels, thereby antagonizing Ca(2+)-driven apoptosis, Cell Death Differ. 29 (2022) 788–805.
[50] M. Kerkhofs, R. La Rovere, K. Welkenhuysen, A. Janssens, P. Vandenberghe, M. Madesh, J.B. Parys, G. Bultynck, BIRD-2, a BH4-domain-targeting peptide of Bcl-2, provokes Bax/Bak-independent cell death in B-cell cancers through mitochondrial Ca(2+)-dependent mPTP opening, Cell Calcium 94 (2021), 102333.
[51] M.E. Young, R.A. Brewer, R.A. Peliciari-Garcia, H.E. Collins, L. He, T.L. Birky, B. W. Peden, E.G. Thompson, B.-J. Ammons, M.S. Bray, J.C. Chatham, A.R. Wende, Q. Yang, C.-W. Chow, T.A. Martino, K.L. Gamble, Cardiomyocyte-specific BMAL1 plays critical roles in metabolism, signaling, and maintenance of contractile function of the heart, J. Biol. Rhythm. 29 (2014) 257–276.
[52] K.A. Ingle, V. Kain, M. Goel, S.D. Prabhu, M.E. Young, G.V. Halade, Cardiomyocyte-specific Bmal1 deletion in mice triggers diastolic dysfunction, extracellular matrix response, and impaired resolution of inflammation, Am. J. Physiol. Heart Circ. Physiol. 309 (2015) H1827–H1836.
[53] M. Lefta, K.S. Campbell, H.-Z. Feng, J.-P. Jin, K.A. Esser, Development of dilated cardiomyopathy in Bmal1-deficient mice, Am. J. Physiol. Heart Circ. Physiol. 303 (2012) H475–H485.